Journal of Glaciology (2018), **64**(244) 343–346 doi: 10.1017/jog.2018.11

Letter

Corrigendum: Spatial and temporal characterisation of sea-ice deformation

Correcting a sign error results in no changes to the key conclusions of Hutchings and others (2011). However, there is an improved agreement with previous work. Mean total sea-ice deformation scales log linearly with distance and the scaling exponent was found to be dependent on time. We find a linear relationship between the temporal scale and spatial scaling exponent, for timescales of an hour to a day. Extrapolating to the timescales of deformation resolved by RADARSAT, we find total deformation and distance scale with an exponent of between −0.16 and −0.19.

1. INTRODUCTION

We present a correction to the calculation of sea-ice deformation presented in Hutchings and others (2011). The figures and interpretation impacted by this correction are identified and discussed. Corroborating results with previous observations of sea-ice deformation, new evidence is presented regarding the compatibility between strain-rate scaling relationships found with drifting buoys (Hutchings and others, 2011, 2012) and RADARSAT data (Marsan and others, 2004).

2. CORRECTION OF STRAIN-RATE CALCULATION

The calculation of strain rate is presented by Hutchings and others (2012). Buoy positions, recorded every 10 min, are linearly interpolated hourly. The hourly positions are used to estimate buoy array area and strain-rate (Fig. 1) following a generalisation of the Kwok (2003) Green's theorem method to use any number of buoys surrounding a deforming region. In Hutchings and others (2011) there is a sign error in the calculation of the strain-rate components $\frac{\partial u}{\partial y}$ and $\frac{\partial v}{\partial y}$. The correct strain components are calculated as:

$$\frac{\partial u}{\partial x} = \frac{1}{2A}\left[\sum_{n=1}^{N-1}(u_{n+1}+u_n)(y_{n+1}-y_n)+(u_1+u_N)(y_1-y_N)\right], \quad (1)$$

$$\frac{\partial u}{\partial y} = -\frac{1}{2A}\left[\sum_{n=1}^{N-1}(u_{n+1}+u_n)(x_{n+1}-x_n)+(u_1+u_N)(x_1-x_N)\right], \quad (2)$$

$$\frac{\partial v}{\partial x} = \frac{1}{2A}\left[\sum_{n=1}^{N-1}(v_{n+1}+v_n)(y_{n+1}-y_n)+(v_1+v_N)(y_1-y_N)\right], \quad (3)$$

$$\frac{\partial v}{\partial y} = -\frac{1}{2A}\left[\sum_{n=1}^{N-1}(v_{n+1}+v_n)(x_{n+1}-x_n)+(v_1+v_N)(x_1-x_N)\right]. \quad (4)$$

Note that the right-hand rule applies and we sum in a counter-clockwise direction, around each buoy array of N buoys, to estimate the line integrals.

These strain-rate components are combined to give divergence, vorticity, pure and normal shear as described in Hutchings and others (2012). The maximum shear strain rate is the resultant of pure and normal shear and does not include the factor of a half shown in Hutchings and others (2012).

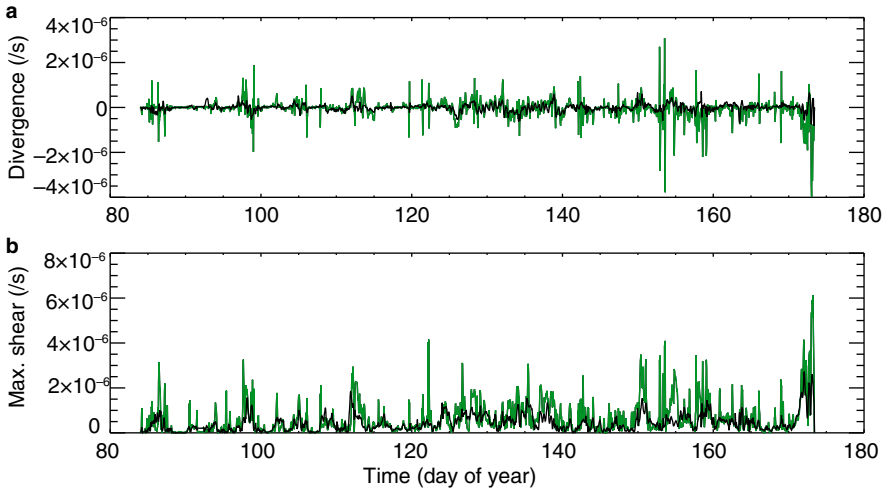

Fig. 1. Corrected Figure 2 in Hutchings and others (2011). Time series of divergence rate (ϵ_I) and maximum shear rate (ϵ_{II}) for the 140 km scale array (black) and 20 km scale array (green). Total deformation rate is calculated as $\sqrt{(\epsilon_I^2+\epsilon_{II}^2)}$.

https://doi.org/10.1017/jog.2018.11 Published online by Cambridge University Press

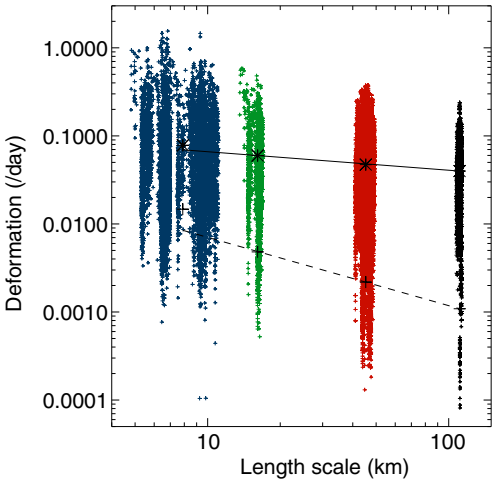

Fig. 2. Corrected Figure 3 in Hutchings and others (2011). All realisations of deformation rate and length scale (square-root of area), for each sub-array in all sets, are plotted in colours corresponding to the length scales they are grouped into. Mean sub-array length scale and mean deformation is plotted (black stars) for each buoy sub-array set. The least squares fit to these values is shown as a solid line. The variance of deformation for each sub-array is plotted (black crosses) and the dashed line is least squares fit to these points.

3. CORRECTED RESULTS

There are subtle differences in several figures resulting from correcting the sign error. These do not affect the interpretation of the data presented in the paper, except in one case. We discuss these differences here.

Figure 2 has a slightly different scaling relationship between total deformation, D, and length scale, L, $D \propto L^H$, with H = −0.21 (reported at H = −0.19 in Hutchings and others (2011)). There are also small differences in the scaling relationship found for other moments of the deformation (Fig. 3).

We still find a small spread in the timescaling for different length scales (Fig. 4). The spectra of total deformation (Fig. 5) demonstrates a spread of behaviour from white noise for the smallest arrays to close to red noise at the 140 km scale. There is no change to the conclusions in the paper regarding the fractal scaling in time varying across length scales.

In spectra of divergence (not shown) a semi-diurnal peak is now apparent. Whereas this does not affect the results presented in this paper, it could have implications to readers interested in sub-diurnal motion of the pack in the Beaufort Sea.

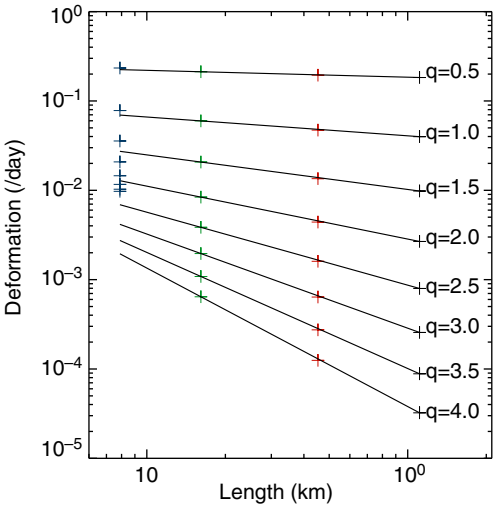

Fig. 3. Corrected Figure 4 in Hutchings and others (2011). Moments (q), between 0.5 and 4, of deformation rate ($<D^q>$), plotted against length scale. The colour of crosses corresponds to length scale as in Figure 2.

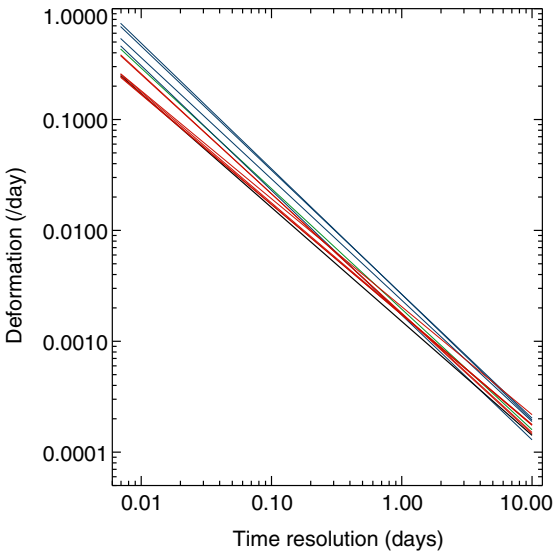

Fig. 4. Corrected Figure 5 in Hutchings and others (2011). Least square fit to the means of deformation rate at each timescale sampled for all SEDNA sub-arrays. The colour corresponds to the spatial scale family, the sub-array belongs to: 10 km blue; 20 km green; 70 km red; and 140 km black. The gradients of the smallest arrays are close to −1.1 and the largest array has a gradient of −1.0.

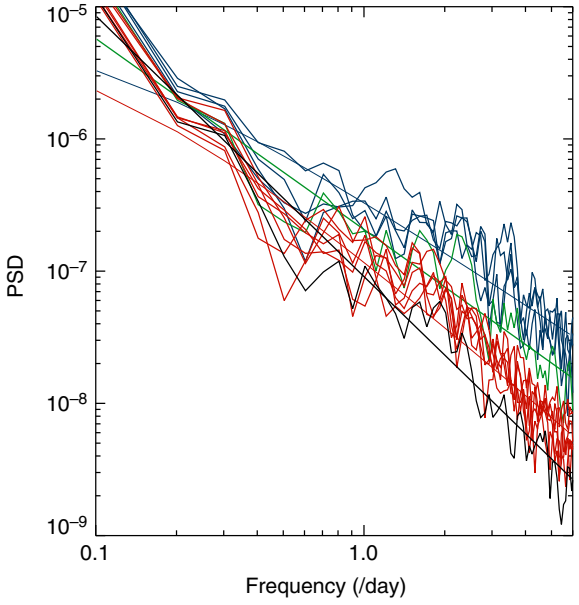

Fig. 5. Corrected Figure 6 in Hutchings and others (2011). Spectral density of deformation for each sub-array, and mean log-log linear fit to spectra with spatial scales of 10 km (blue), 20 km (green), 70 km (red) and 140 km (black) are plotted. At the largest spatial scale, 140 km, the spectra can be approximated by red noise. The other spectra are pink, becoming whiter as spatial scale decreases. At the largest spatial scale, 140 km, the spectra has a slope of −1.97, and this slope decreases with reducing spatial scale: −1.76 (70 km), −1.44 (20 km) and −1.36 (10 km).

https://doi.org/10.1017/jog.2018.11 Published online by Cambridge University Press

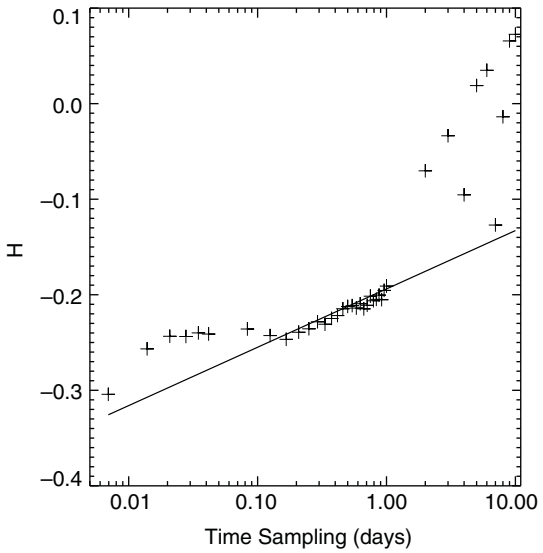

Fig. 6. Corrected Figure 10 in Hutchings and others (2011). Gradients calculated as in Figure 2, for time sampling that varies between 10 min and 10 days. A least square fit to values of H and $log(T)$ is shown. The gradient of this fit is 0.6 logday^{-1}.

The change in gradient of the fit line in Figure 6 is due to the higher scaling exponents at smaller timescales. The linear relationship between space and timescales holds true, as reported before. This relationship when extrapolated to the timescales represented by RADARSAT satellite overpasses, typically 1–3 days, gives H values between −0.16 and −0.19. Previous work using RADARSAT ice-deformation data identified H to be −0.18 (Marsan and others, 2004). Our correction brings our results further in line with previous observations, as the scaling exponent for 1 h deformation is no longer the same as that for the 1–3 day sampling of RADARSAT. This lends confidence to the finding that we can relate the scaling relationships to the temporal scale with a linear relationship in the mean.

Finally, cross correlation between the divergence of the small, inner and large, outer buoy arrays (Fig. 7) displays similar patterns to those reported in Hutchings and others (2011). As before, up until June sea-ice deformation displays coherent deformation between 100 km and the scale of the Beaufort Sea (of order 1000 km) over synoptic time periods. We do find one change: there is no longer a loss of coherence around mid-May. This revised result suggests the transition to a spring ice pack when connectivity is reduced, is occurring in June rather than May and, thus, is happening later and more abruptly than previously shown. The semi-diurnal peak in divergence is increased in the new results, with enhanced coherence on this time period.

4. CONCLUSION

The key finding of Hutchings and others (2011) that deformation at the 10–20 km scale is uncorrelated to the larger scale deformation, is maintained. The identification of fractal scaling of deformation in both time and space is upheld, verifying prior work by Marsan and others (2004) and Rampal and others (2008). The correction allows us to identify a linear relationship between spatial and temporal scaling characteristics over 10–140 km and 1 h to 3 days. This relationship, when extrapolated to between 1 and 3 days agrees with the scaling relationship found for this timescale by Marsan and others (2004). This is a new result, clarifying the coupling of space and timescales identified by Rampal and others (2008).

ACKNOWLEDGMENTS

Many thanks to Polona Itkin and Gunnar Spreen who identified the sign error in our calculations while trying to reproduce our results (Itkin and others, 2017).

[1]*College of Earth Ocean and Atmospheric Sciences, Oregon State University, 104 CEOAS Admin Building, Corvallis, OR 97331, USA,*
[2]*Naval Postgraduate School, Monterey, CA, USA,*
[3]*University of Delaware, Newark, DE, USA,*
[4]*Dartmouth College, Hanover, NH, USA*
[5]*University of Alaska Fairbanks, Fairbanks, AK, USA*

JENNIFER K. HUTCHINGS[1]
ANDREW ROBERTS[2]
CATHLEEN A. GEIGER[3,4]
JACQUELINE RICHTER-MENGE[5]

E-mail: Jennifer K. Hutchings <jhutchings@coas.oregonstate.edu>

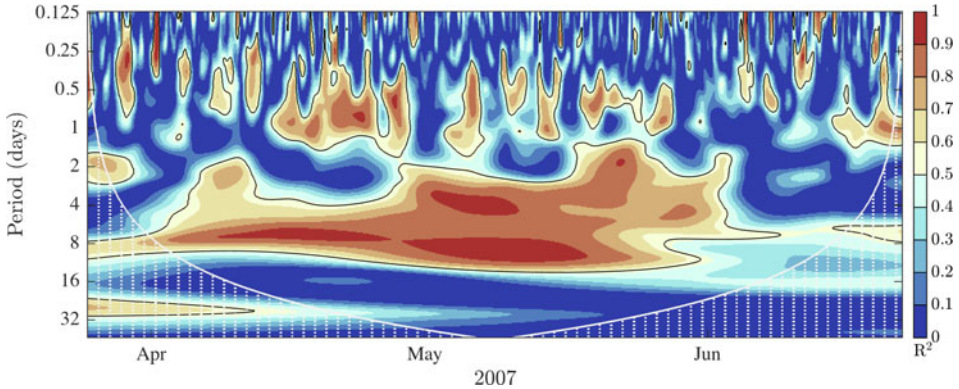

Fig. 7. Corrected Figure 11 in Hutchings and others (2011). The coherence between wavelet spectra of divergence time series for small, 20 km, and large, 140 km buoy arrays. 95% significance levels are encircled by solid black lines. The cone of influence is shown with a bold solid white line, regions outside of this cone indicated by vertical dashed white lines contain data that is likely unrepresentative. 0000Z on 1 May and 1 June are indicated by their month.

https://doi.org/10.1017/jog.2018.11 Published online by Cambridge University Press

REFERENCES

Hutchings JK, Heil P, Steer A and Hibler WD (2012) Subsynoptic scale spatial variability of sea ice deformation in the western Weddell Sea during early summer. *J. Geophys. Res.*, **117**(C1), c01002

Hutchings JK, Roberts A, Geiger CA and Richter-Menge J (2011) Spatial and temporal characterization of sea-ice deformation. *Ann. Glaciol.*, **52**(57), 360–368

Itkin P and 10 others (2017) Thin ice and storms: Sea ice deformation from buoy arrays deployed during N-ICE2015. *J. Geophys. Res.*, **122**(6), 4661–4674

Kwok R (2003) RGPS Arctic Ocean sea ice deformation from SAR ice motion: linear kinematic features Winter 1996–1997, Winter 1997–1998, Summer 1998. *Tech. Rep. JPL D-21524*, Polar Remote Sensing Group, Jet Propulsion Laboratory

Marsan D, Stern H, Lindsay R and Weiss J (2004) Scale dependence and localization of the deformation of Arctic sea ice. *Phys. Rev. Lett.*, **93**(17), 178501

Rampal P, Weiss J, Marsan D, Linday R and Stern H (2008) Scaling properties of sea ice deformation from buoy dispersion analysis. *J. Geophys. Res.*, **113**(C03002) (doi:10.1029/2007JC004143)

MS received 20 November 2017 and accepted in revised form 24 January 2018; first published online 27 March 2018